

# Thermodynamics of chaotic relaxation processes

Domenico Lippolis\*

*School of Mathematical Sciences, Jiangsu University, Zhenjiang 212013, China*

(Dated: July 2, 2024)

The established thermodynamic formalism of chaotic dynamics, valid at statistical equilibrium, is here generalized to systems out of equilibrium, that have yet to relax to a steady state. A relation between information, escape rate, and the phase-space average of an integrated observable (e.g. Lyapunov exponent, diffusion coefficient) is obtained for finite time. Most notably, the thermodynamic treatment may predict the phase-space profile of any integrated observable for finite time, from the leading and subleading eigenfunctions of the Perron-Frobenius/Koopman transfer operator. Examples of that equivalence are shown, and the theory is tested analytically on the Bernoulli map, while numerically on the perturbed cat map, the Hénon map, and the Ikeda map, all paradigms of chaos.

## I. INTRODUCTION

The exponential stretching and folding of phase-space densities that characterizes chaotic dynamics makes long-time evolution unpredictable, and with that the problem of motion intractable. It is then customary to study the statistical properties of the phase space, and in particular to aim at estimating long-time expectation values of relevant observables, under the assumption of asymptotic relaxation of the system to an equilibrium- or a stationary state.

In this framework finds its roots the thermodynamic formalism [1–4], developed from the 1970s on, that is based on the idea of using large-deviation theory [5] to define a dynamical analog of the thermodynamic Gibbs states, which, at statistical equilibrium, do maximize the generating functional of the desired averages, their fluctuations, and multitime correlation functions. This approach is at the basis of the formulation of evolution operators and periodic orbit theory [6], and it has more recently been employed to elucidate the relation between Lyapunov exponents and decay of correlations [7], as well as to identify dynamical phase transitions in deterministic chaos [8–10].

This paper aims at extending the thermodynamic formalism of chaotic dynamics to out-of-equilibrium systems. The Gibbs states of the original formulation are here generalized to include time-dependent weights, later identified with phase-space densities transported by the transfer operator (Perron-Frobenius or Koopman) that governs the time evolution of the system. The so-surmised probabilities for the dynamical microstates give rise to a time-dependent free energy (‘topological pressure’), that is related not only to the finite-time dynamical averages of interest to us, but crucially, to the entire phase-space profiles of the relevant observables.

In the remainder of the present section, I will concisely review the fundamentals and the main results of the thermodynamic formalism of chaotic systems at statistical equilibrium. In section II, I shall extend the key

definition of Gibbs probability for an integrated observable on a chaotic trajectory to a system that has yet to reach equilibrium. Consequently, I derive an expression for finite time, which relates escape rate and Rényi information with free energy (‘topological pressure’) and a newly introduced quantity named tilted information. This non-equilibrium first law approaches the renowned Kantz-Grassberger relation [11] as the system relaxes to equilibrium or a stationary state. Section III contains the main implications of the out-of-equilibrium thermodynamic formalism: any finite-time integrated observable is expressed in terms of the first two eigenfunctions of the Perron-Frobenius- or Koopman operator in a way that its phase-space profile does not depend on the choice of the observable. These claims are validated analytically on the Bernoulli shifts, a paradigm of chaos (Sec. IV A), and numerically on: *i*) the perturbed cat map (Sec. IV B 1), a hyperbolic system defined on a torus, which has no escape and whose transient dynamics is entirely ruled by the second eigenfunction of the transfer operators; *ii*) the Hamiltonian Hénon map (Sec. IV B 2) with weak additive noise, whose dynamics is essentially governed by a chaotic saddle, but it also features an isolated, marginally stable fixed point, which makes the system non-hyperbolic locally.

While the dependence of the out-of-equilibrium observables on the first two eigenfunctions of the transport operator is general, the universality of their profiles breaks down when squeezing is introduced. It is the case of strange attractors, where distinct integrated observables exhibit different phase-space dependence. This is exemplified in Sec. IV B 3 by the noisy Ikeda attractor.

### A. Gibbs states

In the thermodynamics of equilibrium, the entropy  $S$  is maximal when the internal energy  $E$  is fixed (microcanonical ensemble), while the free energy  $F$  is minimized when the internal energy fluctuates (canonical ensemble)

$$F = E - k_B T S. \quad (1)$$

\* domenico@ujs.edu.cn

The Gibbs (canonical) ensemble is made of a number of subsystems, each occurring with a probability  $p_j$ :

$$E = \sum_j p_j E_j \quad (2)$$

$$S = - \sum_j p_j \ln p_j, \quad (3)$$

so that ( $\beta = 1/k_B T$ )

$$F = \sum_j p_j E_j + \frac{1}{\beta} \sum_j p_j \ln p_j. \quad (4)$$

Using Calculus, one can show that the free energy is minimized by choosing [12]

$$p_j = \frac{e^{-\beta E_j}}{\sum_i e^{-\beta E_i}}. \quad (5)$$

Here  $p_j$  is the probability of the subsystem labelled by  $j$  to have energy  $E_j$ . At equilibrium,

$$F_{\min} = - \ln \sum_i e^{-\beta E_i}. \quad (6)$$

The Gibbs formalism has been used to describe chaotic dynamics of ergodic and mixing systems, which, in general do not reach thermodynamic-, but rather statistical equilibrium, asymptotically. Here goes a summary of how that works.

## B. Thermodynamics of chaos

The analysis that follows is formulated for low-dimensional chaotic systems, such as expanding maps on the interval, or hyperbolic Axiom A systems, such as the cat map, whose phase space may be partitioned to a number of distinct regions, and trajectories can be encoded with symbolic sequences [6], tracking the regions visited by each orbit at every instant. In the thermodynamical picture of chaotic dynamics, the phase space is the whole (canonical) ensemble, whose subsystems/Gibbs states are identified with the single (ergodic) trajectories, the latter thought of as infinite sequences in the long-time limit.

In the formalism, the Boltzmann constant  $\beta$  becomes a parameter: given the map  $x_{t+1} = f(x_t)$ , that defines the dynamics, identify the energy with the integrated observable

$$E_j(t) = A_j^t = \sum_{\tau=0}^t a[f^\tau(x_0)], \quad (7)$$

where  $j$  tags the symbolic sequence of the trajectory that starts at  $x_0$  and is iterated by  $\tau$  times by  $f$ , and  $a$  is in general a function of an operator, for example the differential, in the evaluation of the Lyapunov exponents, or the squared position to yield the diffusion constant as

the integrated observable (7). Assuming that the system reaches equilibrium (or a stationary state) for  $t \rightarrow \infty$ , it has been proven [1, 2] that the Gibbs probabilities

$$p_j(t) = \frac{e^{-\beta E_j(t)}}{\sum_i e^{-\beta E_i(t)}} \quad (8)$$

minimize the ‘free energy’, or equivalently, maximize the quantity

$$\mathcal{P}(\beta) = \lim_{t \rightarrow \infty} \frac{1}{t} \ln \sum_j e^{-\beta E_j(t)}, \quad (9)$$

that is known as ‘topological pressure’ [13], although it is in fact a free energy. It has been shown that Eqs. (8)-(9) imply the relation

$$\mathcal{P}(\beta) = \langle A \rangle_\beta + h_\beta, \quad (10)$$

analogous to Eq. (1) for the free energy, where  $\langle \cdot \rangle$  denotes an ensemble average, and

$$h_\beta = - \lim_{t \rightarrow \infty} \frac{1}{t} \frac{1}{\beta - 1} \ln \sum_i p_i^\beta(t) \quad (11)$$

is called Rényi entropy. Equation (10) becomes more familiar when  $\beta = 1$ , and  $\langle A \rangle$  is the positive Lyapunov exponent of the dynamics. In that case,  $\mathcal{P}(1)$  is (minus) the escape rate  $\gamma_0$ , while

$$h_1 = - \lim_{t \rightarrow \infty} \frac{1}{t} \sum_i p_i(t) \ln p_i(t) \quad (12)$$

is the information entropy. One can then write (10) as [3, 11, 14]

$$h_1 = -\gamma_0 + \lambda, \quad (13)$$

that relates information entropy, escape rate, and Lyapunov exponent  $\lambda$ .

## II. FINITE-TIME THERMODYNAMICS

Let us attempt to extend the thermodynamic formalism to finite time, out of equilibrium. I shall begin with a finite-time topological pressure, of the type

$$\mathcal{P}_t(\beta) = \frac{1}{t} \ln \sum_j w_j(t) e^{-\beta A_j^t}, \quad (14)$$

which, technically, may no longer be considered a free energy, since we are now out of equilibrium. The factors  $w_j$  are included in the previous expression for the topological pressure, so that the Gibbs probabilities for every trajectory throughout the Markov partition are now weighed:

$$p_j(t) = \frac{w_j(t) e^{-\beta A_j^t}}{\sum_i w_i(t) e^{-\beta A_i^t}}. \quad (15)$$

At this stage, the previous expression is an Ansatz for the probability of the integrated observable to be  $A_j^t$  in the subsystem (i.e. symbolic sequence) labelled by  $j$ , surmised consistently with the tilted probability (large-deviations) formalism in a dynamics context [15, 16]. The meaning of Eq. (15) will become clearer later on in this section, when the weights  $w_j(t)$  are recognized as phase-space densities transported by the dynamics via the Perron-Frobenius/Koopman operator.

In what follows, I distinguish  $\beta$ , inverse temperature, or more simply variable of the charac-

teristic (moment-generating, partition-) function  $Z_t(\beta) = \sum_j w_j(t) e^{-\beta A_j^t}$ , from  $q$ , order of the Rényi entropy. Then, I use the so-generalized expression for the topological pressure

$$\mathcal{P}_t(q, \beta) = \frac{1}{t} \ln \sum_j w_j^q(t) e^{-q\beta A_j^t}, \quad (16)$$

while it is still understood that  $\mathcal{P}_t(\beta) := \mathcal{P}_t(q = 1, \beta)$ . The Rényi information is the entropy (11) for finite time:

$$\begin{aligned} I_t(q, \beta) &= -\frac{1}{t} \frac{1}{q-1} \ln \sum_i p_i^q(t) = \frac{1}{1-q} \frac{1}{t} \ln \sum_j \frac{w_j^q e^{-q\beta A_j^t}}{[\sum_i w_i e^{-\beta A_i^t}]^q} \\ &= \frac{1}{1-q} \frac{1}{t} \ln \frac{e^{\mathcal{P}_t(q, \beta)t}}{Z_t^q(\beta)} = \frac{1}{1-q} \left[ \mathcal{P}_t(q, \beta) - \frac{1}{t} \ln Z_t^q(\beta) \right]. \end{aligned} \quad (17)$$

The previous can be rewritten as

$$I_t(q, \beta) = \frac{1}{1-q} [\mathcal{P}_t(q, \beta) - q \mathcal{P}_t(\beta)], \quad (18)$$

keeping in mind that everything is time dependent, and out of equilibrium. In the limit  $q \rightarrow 1$ , we have that

$$I_t(1, \beta) = \mathcal{P}_t(\beta) - \mathcal{P}'_t(\beta) = \frac{1}{t} \left[ \ln \sum_j w_j e^{-\beta A_j^t} - \frac{d}{dq} \ln \sum_j w_j^q e^{-q\beta A_j^t} \Big|_{q=1} \right], \quad (19)$$

where

$$\frac{d}{dq} \ln \sum_j w_j^q e^{-q\beta A_j^t} \Big|_{q=1} = \frac{\sum_j w_j e^{-\beta A_j^t} [\ln w_j - \beta A_j^t]}{Z_t(\beta)}. \quad (20)$$

We can already spot three terms in the right-hand side of Eq. (19). The first is simply  $\mathcal{P}_t(\beta)$  with the new definition of weighted probabilities for the symbolic sequences. The second is spelled out in Eq. (20):

$$\frac{1}{t} \frac{\sum_j \beta A_j^t w_j e^{-\beta A_j^t}}{\sum_j w_j e^{-\beta A_j^t}} = \frac{1}{t} \frac{\sum_j \beta p_j(t) A_j^t}{\sum_j p_j(t)} = \beta \langle A^t \rangle_\beta, \quad (21)$$

where the average is taken with respect to the definition (15) of the time-dependent probabilities. In that sense, the previous is a thermodynamic average. The third term in the right-hand side of Eq. (19) I also read out of Eq. (20):

$$\frac{\frac{1}{t} \sum_j w_j \ln w_j e^{-\beta A_j^t}}{\sum_j w_j e^{-\beta A_j^t}} \equiv \frac{S_t(\beta)}{Z_t(\beta)}. \quad (22)$$

This quantity is peculiar of the finite-time thermodynamics, as it was not present in the equilibrium entropy-free energy relation. I name the numerator  $S_t(\beta)$  of

Eq. (22) *tilted information*. Now Eq. (19) takes the form

$$I_t(1, \beta) = \mathcal{P}_t(\beta) + \beta \langle A^t \rangle_\beta - \frac{S_t(\beta)}{Z_t(\beta)}. \quad (23)$$

Equation (23) is the first result of this paper: it generalizes the known asymptotic relation (10) between information entropy, topological pressure, and expectation of an integrated observable to finite-time chaotic dynamics, out of statistical equilibrium. Besides the quantities mentioned, the term  $S_t$  newly appears in the equation: it represents the information provided by the weights  $w_j$ , biased by the Gibbs probabilities  $e^{-\beta A_j^t}$  of the integrated observable. This additional term must be transient, that

is it must vanish as  $t \rightarrow \infty$ , when the whole expression (23) approaches the equilibrium identity (10), as shown in Appendix A.

At first sight, Eq. (23) does not bear physical significance beyond that of its equilibrium counterpart, nor does it have ostensible implications or use. Yet, all the quantities involved are now defined in terms of the time-dependent statistical weights  $w_j$ , that will play a central role in the non-equilibrium statistics of the integrated observables  $A^t$ , as shown in Sec. III.

Let us now identify the weights  $w_j$ . This task is best accomplished by taking as integrated observable the finite-time Lyapunov exponent

$$A^t = \ln ||J^t(x_0)|| = \ln |\Lambda(t)|, \quad (24)$$

where the Jacobian is defined as

$$J_{ij}^t(x) = \frac{\partial f_i^t(x)}{\partial x_j}. \quad (25)$$

The regions of a given partition are evolved by the dynamics, in such a way that the total probability (measure) is conserved at every time step:

$$p_j(t) = \sum_i p_i(t+1). \quad (26)$$

Using our hypothesis (15) for the  $p_i$ 's, the previous identity would translate to the evolution

$$\frac{w_j(t)}{|\Lambda_j(t)|^\beta} = e^{-\mathcal{P}_t(\beta)} \sum_i \frac{w_i(t+1)}{|\Lambda_i(t+1)|^\beta}, \quad (27)$$

once we write the probability of every partition element in terms of the stability exponent as integrated observable [Eq. (24)]. This evolution can be written in terms of the Perron-Frobenius operator [7], where we consider the  $w_j$ 's as densities. For a one-dimensional map, that reads

$$\rho'(x_j) = e^{-\mathcal{P}_t(\beta)} \sum_i \frac{\rho(x_i)}{|f'(x_i)|^\beta}. \quad (28)$$

That identifies the  $w_j(t)$ 's with time-varying densities.

Now, look at Eq. (27): going from time  $t$  to time  $t+1$  means to extend every interval of a Markov partition by one symbol. For instance, if the symbolic dynamics is binary, that is the phase space is partitioned into two regions coded by 0 and 1, we let  $t=3$  and, say,  $j=001$ , then  $t+1=4$  and the terms of the summation on the right-hand side are  $i=0010, 0011$ . In that case, the densities  $w_j$ 's map forward as stated by the 'Perron-Frobenius' equation (27). If we decide to stop at some definite  $t$  and identify the set of all the distinct trajectories with a Markov partition, the  $p_j$ 's are given by the thermodynamic expression (15), where the  $w_j$ 's are the densities in each interval of the partition. Therefore, the  $w_j$ 's are the probabilities of the dynamics to visit each region of the partition, or, equivalently, the probabilities of

each trajectory, whereas the  $p_j$ 's are the probabilities for region (sequence)  $j$  to measure the observable  $A_j^t$ , and, for finite time, they ought to be weighed by  $w_j$ , even if the dynamical system  $f$  is ergodic and mixing.

Remarks are in order about the finite-time average and topological pressure. First, for  $A^t = \ln |\Lambda(t)|$ , the finite-time thermodynamic average (21) becomes

$$\langle \ln |\Lambda(t)| \rangle_\beta = \frac{\sum_j w_j(t) \ln \Lambda_j(t) / \Lambda_j^\beta(t)}{\sum_j w_j(t) / \Lambda_j^\beta(t)}, \quad (29)$$

which makes sense dynamically, if we recall that the neighborhood of each region of a Markov partition of  $t$  regions scales as  $1/|\Lambda_j(t)|^d$  in a hyperbolic system [3]. That way, Eq. (29) may be regarded as a weighed average over the partition.

On the other hand, the finite-time topological pressure may be reconnected to more familiar quantities such as the moment-generating function in a continuous phase space, where it is written as

$$\begin{aligned} \mathcal{P}_t(\beta) &= \frac{1}{t} \ln \sum_j w_j(t) e^{-\beta A_j^t} \\ &\rightarrow \frac{1}{t} \ln \int dx w(x(t)) e^{-\beta A^t(x)} = \frac{1}{t} \ln \langle e^{-\beta A^t} \rangle, \end{aligned} \quad (30)$$

where the first identity holds in the limit of an infinitely fine partition, with every point in the phase space belonging to a distinct sequence of  $t$  symbols, while the derivatives of  $\langle e^{-\beta A^t} \rangle$  with respect to  $\beta$  are the moments of the observable  $A^t$  weighed by  $w(x(t))$  [6]. One may then rewrite Eq. (23) as

$$I_t(1, \beta) = \frac{1}{t} \ln \langle e^{-\beta A} \rangle + \beta \langle A^t \rangle_\beta - \frac{S_t(\beta)}{Z_t(\beta)}, \quad (31)$$

recalling that  $I_1(\beta)$  and the last two terms do carry a prefactor of  $1/t$  in their definitions.

Expressing the probability weights  $w$  as phase-space densities in the continuum limit is central in the evaluation of the finite-time averages of the integrated observables, as exposed in what follows.

### III. AVERAGES

In this finite-time thermodynamic picture, an average is taken as in Eq. (21), with the numerator of that expression being

$$\sum_j A_j^t w_j e^{-\beta A_j^t}. \quad (32)$$

The index  $j$  refers to a particular orbit, identified with a symbolic sequence, and thus to a family of trajectories

that share the same itinerary throughout the partition up to time  $t$ . First, recall the definition (7)

$$A^t(x) = \sum_{\tau=0}^t a[f^\tau(x)]. \quad (7)$$

For a long sequence in a Markov partition, I shall approximate the sum over sequences with an integral over the phase space, as seen in Eq. (30). In the phase-space analog of Eq. (32), I can either choose  $w$  to be computed at  $t = 0$ , or at a later  $t$ . In the former case, the average may be written

$$\int dx A^t(x) w(x) e^{-\beta A^t(x)}, \quad (33)$$

whereas in the latter, the integrated observable follows the family of trajectories  $f^{-t}(x) \rightarrow x$  [17], so that

$$\int dx A^t(f^{-t}(x)) e^{-\beta A^t(f^{-t}(x))} [\mathcal{L}_t w](x), \quad (34)$$

where the Perron-Frobenius evolution operator acts as

$$\begin{aligned} (\mathcal{L}_t \cdot w)(x) &= \int dy \delta(x - f^t(y)) w(y) = \\ &= \sum_{x_0=f^{-t}(x)} \frac{w(x_0)}{|\det J^t(x_0)|}. \end{aligned} \quad (35)$$

## A. Going forward

Let us first study the average with the weight function evaluated at time  $t$ , as in Eq. (34), while Eq. (33) with the density evaluated at time zero will be considered in Sec. III C. Assuming a discrete spectrum for the Perron-Frobenius operator, the goal is now to express the average

$$\langle A^t \rangle_\beta = \frac{\int dx A^t(f^{-t}(x)) e^{-\beta A^t(f^{-t}(x))} [\mathcal{L}_t w](x)}{\int dx e^{-\beta A^t(f^{-t}(x))} [\mathcal{L}_t w](x)} \quad (36)$$

in terms of the leading eigenfunctions of  $\mathcal{L}^t$ .

In Eq. (34) I now expand  $\mathcal{L}_t w$ , obtaining

$$\int dx A^t(f^{-t}(x)) e^{-\beta A^t(f^{-t}(x))} [\mathcal{L}_t w](x) = \sum_n^\infty b_n e^{-\gamma_n t} \int dx \phi_n(x) A^t(f^{-t}(x)) e^{-\beta A^t(f^{-t}(x))}, \quad (37)$$

where  $e^{-\gamma_n t}$  and  $\phi_n(x)$  are respectively eigenvalues and eigenfunctions of the Perron-Frobenius operator  $\mathcal{L}_t$ , while

$$b_n = \int w(y) \varphi_n(y) dy \quad (38)$$

are the coefficients of the expansion, that depend on the initial densities  $w(x)$  and the eigenfunctions  $\varphi_n$  of the Koopman operator  $\mathcal{L}_t^\dagger$ . Let us then go back to the original thermodynamic average (36), and rewrite it harnessing the above expansion:

$$\langle A^t \rangle_\beta = \frac{\sum_n^\infty b_n e^{-\gamma_n t} \int dx \phi_n(x) A^t(f^{-t}(x)) e^{-\beta A^t(f^{-t}(x))}}{\sum_n^\infty b_n e^{-\gamma_n t} \int dx \phi_n(x) e^{-\beta A^t(f^{-t}(x))}}. \quad (39)$$

Now let  $\beta = 0$ :

$$\langle A^t \rangle_{\beta=0} = \frac{\sum_n^\infty b_n e^{-\gamma_n t} \int dx \phi_n(x) A^t(f^{-t}(x))}{\sum_n^\infty b_n e^{-\gamma_n t} \int dx \phi_n(x)}. \quad (40)$$

It is the expansion of an average, and perhaps that does not say much per se. However, we may recover the original expression for  $A^t$  and focus on its phase-space dependence, if we start with an initial density of the type  $w(y) = \delta(y - x_0)$ , that is concentrated in one point:

$$\langle A^t \rangle_{\beta=0}(x_0) = \frac{\int dx A^t(f^{-t}(x)) \int dy \delta(x - f^t(y)) \delta(y - x_0)}{\int dx \int dy \delta(x - f^t(y)) \delta(y - x_0)} = \frac{A^t(x_0)}{\mu(\mathcal{M}(t))} =: \hat{A}^t(x_0), \quad (41)$$

where  $\mu(\mathcal{M}(t))$  is the fraction of trajectories that do not escape after time  $t$ , and it equals unity for a closed system. Concerning the expansion (39), the coefficients  $b_n$  defined by Eq. (38) simply equal  $\varphi_n(x_0)$  when  $w(x) = \delta(x - x_0)$ ,

and the integrated observable spells

$$\langle A^t \rangle_{\beta=0}(x_0) = \hat{A}^t(x_0) = \frac{\sum_n^\infty \varphi_n(x_0) e^{-\gamma_n t} \int dx \phi_n(x) A^t(f^{-t}(x))}{\sum_n^\infty \varphi_n(x_0) e^{-\gamma_n t} \int dx \phi_n(x)}. \quad (42)$$

In the limit  $t \rightarrow \infty$ , only the first term survives

$$\langle A^t \rangle_{\beta=0}(x_0) \rightarrow \frac{\int dx \phi_0(x) A^t(f^{-t}(x))}{\int dx \phi_0(x)}, \quad (43)$$

that is simply the phase-space average weighed by the invariant density  $\phi_0(x)$ , as it is known at equilibrium, and the dependence on  $x_0$  has been lost. The interesting time scale in the present context is rather that of  $(\gamma_1 - \gamma_0)^{-1}$ , at which the expanded average (42) is approximately

$$\hat{A}^t(x_0) := \langle A^t \rangle_{\beta=0}(x_0) \simeq \int_{\mathcal{M}} A^t(f^{-t}(x)) \phi_0(x) dx + \frac{\varphi_1(x_0)}{\varphi_0(x_0)} e^{-(\gamma_1 - \gamma_0)t} \int_{\mathcal{M}} A^t(f^{-t}(x)) \phi_1(x) dx. \quad (44)$$

Now assume that the system has no escape. We may take the natural measure  $\phi_0(x)$  to be  $L^1$ -normalized in the phase space, while the other eigenfunctions of the Perron-Frobenius operator are such that  $\int dx \phi_n(x) = 0$ . That way, the previous expression for the ‘pointwise average’ becomes

$$\hat{A}^t(x_0) \simeq \langle A^t \rangle_{\mathcal{M}} + \varphi_1(x_0) e^{-\gamma_1 t} \int dx \phi_1(x) A^t(f^{-t}(x)), \quad (45)$$

where  $\langle A^t \rangle_{\mathcal{M}} = \int dx \phi_0(x) A^t(f^{-t}(x))$ . In case of no escape ( $\gamma_0 = 0$ ), the ground state of the Koopman operator is a uniform distribution, since

$$\mathcal{L}_t^\dagger \varphi_0(x) = \varphi_0(f^t(x)) = \varphi_0(x) \quad (46)$$

for every  $x$ , whence  $\varphi_0(x) = 1$  in Eq. (45).

Equation (45) tells us that the phase-space profile of the integrated observable  $A^t$  is entirely ruled by the sub-leading eigenfunction  $\varphi_1(x)$  of the Koopman operator at the time scale  $1/\gamma_1$ , which determines  $\hat{A}^t(x_0)$  independently of the observable itself.

## B. Perron-Frobenius vs. Koopman operator

The Perron-Frobenius operator  $\mathcal{L}_t$  carries a density  $\rho$ , supported on  $\mathcal{M}$ , forward in time to a density supported on a subset of  $f^t(\mathcal{M})$  [18]. In this sense,  $\mathcal{L}_t$  ‘follows the flow’. On the other hand, the Koopman operator  $\mathcal{L}_t^\dagger$  acts as

$$\mathcal{L}_t^\dagger \rho(x) = \rho(f^t(x)), \quad (47)$$

and so

$$\rho(f^t(x)) = 0 \quad \text{if } f^t(x) \notin \mathcal{M}. \quad (48)$$

That implies that

$$\mathcal{L}_t^\dagger \rho(x) = 0 \quad \text{if } x \notin f^{-t}(\mathcal{M}), \quad (49)$$

meaning that the the Koopman operator is supported on the preimage of the set  $\mathcal{M}$ , and thus  $\mathcal{L}_t^\dagger$  may be thought of as transporting a density supported on  $\mathcal{M}$  backward in time to a density supported on  $f^{-t}(\mathcal{M})$ .

## C. Going backward : a matter of pinning

But why is the field profile of the integrated observable  $A^t$  governed by the eigenfunctions of the Koopman operator, and not by those of its adjoint, the Perron-Frobenius operator? The reason is that in Eq. (34)  $x$  is the final point of the density  $w$  and of the integrated observable  $A^t$ . If, on the contrary, I had chosen to pinpoint density and observable by their values at the initial point of the trajectory originally labelled by the symbolic sequence  $j$  in the discretized state space, I could have written  $w$  as an evolution by the Koopman operator:

$$w(f^t(x)) = \int dy \delta(y - f^t(x)) w(y). \quad (50)$$

Then, the course of action leading to the expansion of the average (39) is ‘adjointed’. Let us use the definition (7) for the integrated observable as a function of  $x_0$ , that is the initial point, and rewrite Eq. (33) with observable and density still a function of the initial point  $x$ :

$$\int dx A^t(x) e^{-\beta A^t(x)} \left[ \mathcal{L}_t^\dagger w \right] (x) = \int dx e^{-\beta A^t(x)} A^t(x) \int dy \delta(y - f^t(x)) w(y), \quad (51)$$

The density evolution in the left-hand side of (51) is then

expanded in terms of the eigenspectrum of the Koop-



man operator  $\mathcal{L}_t^\dagger$ , as done in Eq. (37) for the Perron-Frobenius operator. As imaginable, the average of  $A^t$  is now ‘dual’ to the expression (39), with the eigenfunctions  $\varphi_j$  of the Koopman operator replacing those of the Perron-Frobenius operator. Subsequently, I pin the ini-

$$\hat{A}^{-t}(x_t) := \frac{A^t(f^{-t}(x_t))}{\mu(\mathcal{M}(t))|\det J^t(f^{-t}(x_t))|} \simeq \int_{\mathcal{M}} A^t(x)\varphi_0(x) dx + \frac{\phi_1(x_t)}{\phi_0(x_t)} e^{-(\gamma_1-\gamma_0)t} \int_{\mathcal{M}} A^t(x)\varphi_1(x) dx. \quad (52)$$

The previous expression is akin to Eq. (44), and it only but importantly differs in the variable of our choice (the arrival point of each phase-space trajectory, as opposed to the starting point in Eq. (44)), as well as in the eigenfunctions of  $\mathcal{L}_t$ , rather than those of  $\mathcal{L}_t^\dagger$ .

#### D. Evolution on the manifold

An argument was presented in [19, 20] to show that the evolution of a density by the Perron-Frobenius operator along the unstable manifold of an area-preserving, fully chaotic map leads to the following result: the distribution of the finite-time Lyapunov exponents in the phase space (the unit torus) follows the pattern of the second eigenfunction of the Perron-Frobenius operator, at a suitable time scale. The idea is that, on the unstable manifold, the Perron-Frobenius operator acts on a density as

$$\mathcal{L}_t w(x) \sim e^{-t\Lambda(f^{-t}(x),t)} w(x), \quad (53)$$

where the Lyapunov trajectory begins at  $f^{-t}(x)$  and runs for time  $t$  up to  $x$ . On the other hand, as seen, the action of the Perron-Frobenius operator on the same density may be expanded and truncated as (assuming no escape)

$$\mathcal{L}_t w(x) = c_0 + c_1 e^{-\gamma_1 t} \phi_1(x) + O(e^{-\gamma_2 t}). \quad (54)$$

Along the unstable manifold, the evolution is thus linearized as in Eq. (53), and so it does not depend on  $w(x)$ , but only on the finite-time Lyapunov exponent  $e^{-\Lambda(f^{-t}(x),t)}$ , whose phase-space profile should then fol-

low  $\phi_1(x)$  at a time scale set by  $\gamma_1^{-1}$ :

$$e^{-t\Lambda(f^{-t}(x),t)} \propto \phi_1(x) e^{-\gamma_1 t}, \quad (55)$$

meaning that the second eigenfunction of the Perron-Frobenius operator rules the distribution of the finite-time Lyapunov exponents pinned at the final point of each trajectory. That is consistent with Eq. (52), which generalizes the theory to an arbitrary observable (one would use Eq. (44) when pinning the observable at the initial point of each iterated trajectory, instead).

#### E. Noise

The finite-time thermodynamic formalism exposed in the previous section may also describe a chaotic system with background noise, according to the evolution

$$x_{t+1} = f(x_t) + \eta(t) := f_\eta(x_t), \quad (56)$$

with random force  $\eta(t)$ . The integrated observable (7) would now take the form

$$A_{\sigma^2}^t(x_0) = \left\langle \sum_{\tau=0}^t a(f_\eta^\tau(x_0)) \right\rangle_{\sigma^2}, \quad (57)$$

where  $\langle \cdot \rangle_{\sigma^2}$  denotes an ensemble average over noisy trajectories  $f_\eta^t(x)$ , with isotropic noise of amplitude  $2\sigma^2$ . In this setting, phase-space densities are transported by an evolution operator with a noisy kernel, for example the Fokker-Planck operator [21], applied at each iteration:

$$[\mathcal{L}_{\sigma^2} w](x) = \frac{1}{\sqrt{4\pi\sigma^2}} \int dx e^{-(y-f(x))^2/4\sigma^2} w(x). \quad (58)$$

With that change, Eq. (42) would become, in the noisy phase space,

$$\langle A^t \rangle_{\beta=0}(x_0) = \frac{A_{\sigma^2}^t(x_0)}{|\mathcal{M}_{\sigma^2}(t)|} = \frac{\sum_n^\infty \varphi_n(x_0) e^{-\gamma_n t} \int dx \phi_n(x) A_{\sigma^2}^t(f^{-t}(x))}{\sum_n^\infty \varphi_n(x_0) e^{-\gamma_n t}}. \quad (59)$$

Now  $\phi$  and  $\varphi$  are respectively right and left eigenfunctions of the Fokker-Planck operator (58), that retains

the spectral gap of the Perron-Frobenius operator, under the same assumptions as in the deterministic picture.

## IV. VALIDATION

The above predictions are now tested on different models of chaos, namely the Bernoulli map, the perturbed cat map, the noisy Hamiltonian Hénon map, and the noisy Ikeda map.

### A. Bernoulli map

It is defined as

$$f(x) = 2x \bmod 1 = \begin{cases} 2x & 0 \leq x < \frac{1}{2} \\ 2x - 1 & \frac{1}{2} \leq x < 1. \end{cases} \quad (60)$$

This one-dimensional, non-invertible map, features chaos everywhere on the unit interval, no escape, and it has a constant Lyapunov exponent equal to  $\ln 2$ .

The spectra of both the Perron-Frobenius and the Koopman operators are discrete with  $L^2$  as function space [22], and available analytically. The Perron-Frobenius operator acts on a density at each time step as

$$\mathcal{L}\rho(x) = \frac{1}{2} \left[ \rho\left(\frac{x}{2}\right) + \rho\left(\frac{x+1}{2}\right) \right], \quad (61)$$

and it has the Bernoulli polynomials

$$\phi_0(x) = 1 \quad (62)$$

$$\phi_1(x) = x - \frac{1}{2} \quad (63)$$

$$\phi_2(x) = x^2 - x + \frac{1}{6} \quad (64)$$

...

as eigenfunctions of eigenvalues  $\gamma_n = 2^{-n}$ . The one-dimensional nature of the phase space makes the forward action (61) all expanding, while the backward, Koopman operator [23]

$$\mathcal{L}^\dagger \rho(x) = \rho(2x)\Theta\left(\frac{1}{2} - x\right) + \rho(2x-1)\Theta\left(x - \frac{1}{2}\right), \quad (65)$$

is everywhere squeezing (here  $\Theta$  is the Heaviside step function). Its leading eigenfunction  $\varphi_0(x) = 1$  is again uniform on the unit interval, while the rest of the spectrum is made of the generalized functions

$$\varphi_j(x) = \frac{(-1)^{j-1}}{j!} \left[ \delta_-^{j-1}(x-1) - \delta_+^{j-1}(x) \right], \quad (66)$$

for  $j \geq 1$ , that is combinations of Dirac delta functions and their derivatives. This behavior is peculiar of one-dimensional chaotic maps. Due to the result (66), we may not apply the expansion (44), that yields an integrated observable  $\hat{A}^t(x)$  in terms of the first two eigenfunctions  $\varphi_0$  and  $\varphi_1$  of the Koopman operator, since the present theory assumes the  $\varphi_i$ 's to be smooth. Instead,

we may test the validity of the expression (52), that relates the polynomial eigenfunctions (64) to the integrated observable  $\hat{A}^{-t}(x)$ , pinned by the final points of the orbits  $f^{-t}(x) \rightarrow x$ .

I shall now take two test observables,  $a_1(x) = x^2$ , and  $a_2(x) = x + \sin 20x$ , apply the Perron-Frobenius operator (61) and integrate the outcomes over a finite time interval. Applying  $\mathcal{L}_t$  has the effect of progressively

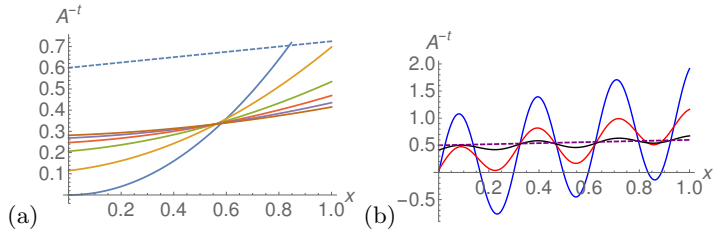


FIG. 1. Test observables mapped by the Perron-Frobenius operator and time integrated: (a)  $a_1 = x^2$  (blue, solid line) and successive  $\hat{A}_1^{-t}(x)$  (solid lines in color) with  $t = 3, t = 5, t = 8, t = 10, t = 15$  approaching a straight line (for increasing  $t$ ), plotted above (dashed line) for comparison; (b)  $a_2 = x + \sin 20x$  (blue, solid line), and successive  $\hat{A}_2^{-t}(x)$  (solid lines in color) with  $t = 8, t = 15$  approaching a straight line (dashed line).

smoothing observables as  $t$  increases, e.g.

$$[\mathcal{L}_{t=5}a_1](x) = 0.3 + 0.06x + 0.004x^2, \quad (67)$$

or

$$[\mathcal{L}_{t=5}a_2](x) = 0.46 + 0.14x + 0.002x^2 + O(x^3), \quad (68)$$

when expanding the closed-form expression of  $[\mathcal{L}_{t=5}a_2](x)$  in a power series. As a consequence, the mapping of both  $a_1, a_2$  produces curves that are approximately straight, and, at a longer timescale, the corresponding integrated observables  $\hat{A}_1^{-t}, \hat{A}_2^{-t}$ , also approach the functional form of the second eigenfunction of the Perron-Frobenius spectrum (Fig. 1),  $\phi_1(x) = x - \frac{1}{2}$ . Specifically, Eq. (52) predicts that  $\hat{A}^{-t}(x) \sim \phi_1(x)/\phi_0(x)$ , where  $\phi_0(x) = 1$  in this case, while the proportionality factor (slope of the line) depends on the observable.

### B. Two-dimensional maps

The strategy is that to numerically compute the first two eigenfunctions of the Perron-Frobenius and of the Koopman spectrum, and compare their ratio with the phase-space profiles of different integrated observables for finite time.

The leading- and subleading eigenfunctions of the Perron-Frobenius/Koopman operator are first computed as follows. The transfer operator is projected onto a finite-dimensional vector space, and thus implemented as a matrix, as it is by now common when solving flow



(e. g. Liouville [24]) equations. Previous literature warns us that the choice of the discretization is crucial [25], and may deeply affect the eigenspectrum beyond the leading eigenvalue [26]. It has been established, on the other hand, that nonlinear perturbations to linear maps on a torus increase the robustness of the numerically evaluated spectrum under certain conditions [27]. The simplest discretization scheme is Ulam's method [28], that amounts to subdividing the phase space into  $N$  intervals  $\mathcal{M}_i$  of equal area. The evolution operator is thus approximated with a  $N \times N$  transfer matrix whose entries  $\mathbf{L}_{ij}$  are the transition probabilities from  $\mathcal{M}_i$  to  $\mathcal{M}_j$

$$\mathbf{L}_{ij} = \frac{\mu(\mathcal{M}_i \cap f^t(\mathcal{M}_j))}{\mu(\mathcal{M}_i)} \quad (69)$$

in one time step, where  $\mu$  is the Lebesgue measure. I use a known Monte Carlo method [29] to estimate the nonsymmetric transfer matrix  $\mathbf{L}_{ij}$ , that consists of iterating random initial conditions from each cell  $\mathcal{M}_i$  and counting which fraction lands in each  $\mathcal{M}_j$ . A thorough study of stability and convergence of discretization algorithms has been reported elsewhere by the author and co-workers [20], among others.

### 1. Perturbed cat map

The first two-dimensional model considered is the perturbed cat map  $f(x) = T_\epsilon \circ T[x]$ , with  $x = (q, p)$ :

$$T \begin{pmatrix} q \\ p \end{pmatrix} = \begin{pmatrix} 1 & 1 \\ 1 & 2 \end{pmatrix} \begin{pmatrix} q \\ p \end{pmatrix} \mod 1, \quad (70)$$

and

$$T_\epsilon \begin{pmatrix} q \\ p \end{pmatrix} = \begin{pmatrix} q - \epsilon \sin 2\pi p \\ p \end{pmatrix} \mod 1. \quad (71)$$

This system is strongly chaotic and hyperbolic, that is,

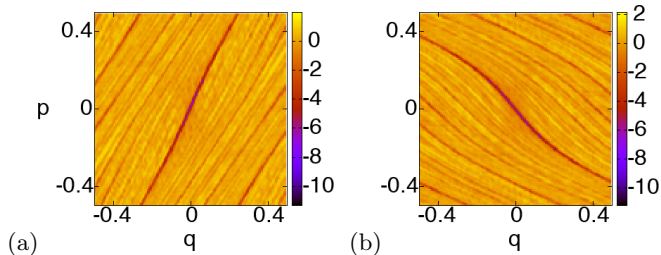


FIG. 2. First subleading eigenfunctions of the (a) Perron-Frobenius- and (b) Koopman operator for the perturbed cat map. The Ulam matrix has size  $2^{14} \times 2^{14}$ .

correlations decay exponentially fast with time [30]. It possesses an infinite number of unstable periodic orbits, and, specifically, a fixed point at the origin. The phase space is a 2-torus, there is no escape, and areas are preserved by the time evolution, so that the determinant

of the Jacobian matrix of every trajectory is equal to unity. I set the parameter  $\epsilon = 0.1$  in what follows, a small enough value for the topology of the phase space to be preserved, yet large enough for the nonlinearity (71) to make the Ulam discretization robust.

The leading eigenfunctions of the transfer operators for the cat map are uniform distributions, and therefore they will not affect the predictions of the present theory out of equilibrium. Instead, the subleading eigenfunctions of the Perron-Frobenius and Koopman operators, computed with the Ulam method, are shown in Fig. 2.

Here, I first verify prediction (45) for an integrated observable pinned by its initial point in the phase space,  $A^t(x_0)$ . The observables employed here are

1. The finite-time Lyapunov exponent (24) of the cat map.
2. The average diffusion

$$\overline{D}^t(x) = \frac{1}{t} \sum_{\tau=0}^t q^2(f^\tau(x)), \quad (72)$$

with  $t \sim \gamma_1^{-1}$ .

3. The average kinetic energy

$$\overline{K}^t(x) = \frac{1}{t} \sum_{\tau=0}^t \frac{p^2(f^\tau(x))}{2}, \quad (73)$$

again with  $t \sim \gamma_1^{-1}$ .

The desired finite-time density plots are obtained by iterating some  $10^8$  randomly chosen, uniformly distributed initial conditions until a time  $t$  before relaxation. The outcomes are shown in Fig. 3: all the observables are striated along the stable manifold, and, in particular, their profiles are all alike, and their features echo with those of the first subleading eigenfunction of the Koopman operator [Fig. 2(b)]. Enhancement ('scar') of the latter [19] corresponds to suppression ('antiscar') of the integrated observable, which is ascribed to the second term of Eq. (45): it is found that either  $\varphi_1(x_0) < 0$  and maximally negative at the scar with the integral  $\int dx \phi_1(x) A^t(f^{-t})(x) > 0$  (from numerics), or vice versa [31], and so the pointwise value of the integrated observable  $\hat{A}^t$  is approximately given by a constant (its phase-space average) *minus* something proportional to the second eigenfunction of the Koopman operator. As a result, a scar in the second eigenfunction produces an antiscar in the density plots of all integrated observables at time scale  $\gamma_1^{-1}$ , as apparent in Fig. 3.

Let me now proceed speculatively with the validation of the prediction (52) of an integrated observable pinned by its final point (iteration at time  $t$ ) in the phase space,  $\hat{A}^{-t}(x_t)$ . The tested observables are once again the finite-time Lyapunov exponent, the average diffusion, and the kinetic energy. The results are displayed in Fig. 4, and are analogous to what seen with the initial-point pinning,

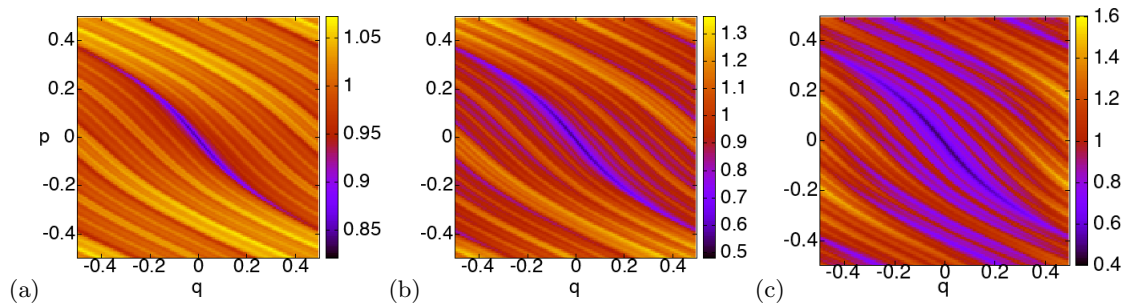


FIG. 3. Phase-space density plots ( $2^{14}$  points, each averaged over  $10^4$  trajectories) of (a) the finite-time Lyapunov exponents, (b) the integrated kinetic energy, (c) the average diffusion, of the perturbed cat map having the  $(q, p)$  coordinates as initial points. The map is iterated until time  $t = 15$ .

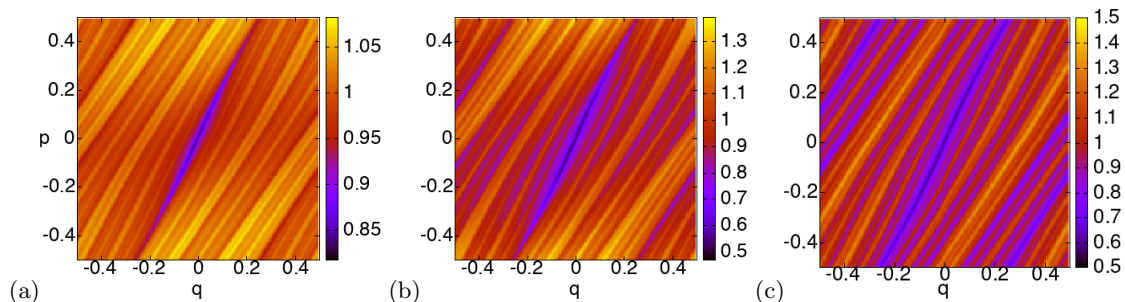


FIG. 4. Same as Fig. 3, but here  $(q, p)$  are the coordinates of the \*final\* points.

except that all the profiles are striated along the unstable manifold of the map, and follow the second eigenfunction of the Perron-Frobenius operator [Fig. 2(a)], here denoted by  $\phi_1(x)$ . The equivalence between eigenfunction enhancement and observable suppression is still verified in this case, as one can infer from Eq. (52).

In order to quantify the similarities between distinct finite-time observables, Fig. 5 portrays the density plot of the logarithmic ratio

$$r(x_0, t) = \ln \left| \frac{\ln |\Lambda(x_0, t)| - \langle \ln |\lambda(x, t)| \rangle_{\mathcal{M}}}{\overline{D}(x_0, t) - \langle \overline{D}(x, t) \rangle_{\mathcal{M}}} \right| \quad (74)$$

between the diffusion and the Lyapunov exponent, scaled by their mean values, both in the Perron-Frobenius and in the Koopman pictures of pinpointing. If the present theory holds, we should expect  $r(x, t)$  to be a uniform distribution plus or minus fluctuations, and indeed the plots give that indication.

## 2. Hamiltonian Hénon map

The next model to test the theory on is the Hamiltonian Hénon map

$$\begin{aligned} q' &= 1 - \alpha q^2 + \beta p \\ p' &= q, \end{aligned} \quad (75)$$

with  $\alpha = 1.4$  and  $\beta = -1$ . This choice of the parameters avoids dissipation in the dynamics ( $|\beta| = 1$ ), but

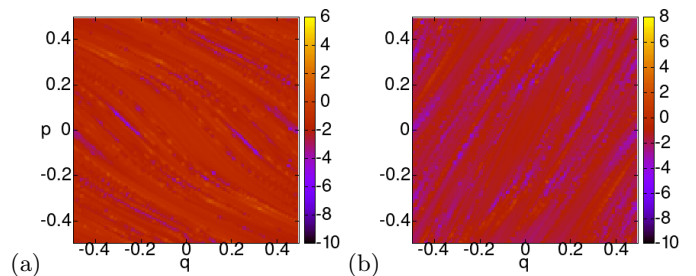


FIG. 5. The logarithmic ratio (74) between ( $2^{14}$  points) the finite-time Lyapunov exponents and the integrated kinetic energy, for the perturbed cat map having the  $(q, p)$  coordinates as (a) initial- and (b) final points. The map is iterated until time  $t = 15$ .

it offers a new scenario to validate the present theory, due to: *i*) escape to infinity from the neighborhood of the hyperbolic fixed point  $x_p \simeq (-1.1, -1.89)$ , that generates a chaotic saddle through its stable and unstable manifolds (the latter is portrayed in Fig. 6(a)); *ii*) a not-everywhere chaotic but rather mixed phase space, given the presence of a second fixed point,  $x_c \simeq (0.39, 0.39)$ , that is marginally stable, and surrounded by a small non-hyperbolic region (Fig. 6(b)). In order to ‘kick’ the dynamics out of the latter non-chaotic region and into the chaotic phase, weak noise is added to the map (75) of an amplitude comparable to the size of the stability island per unit time.

Strictly speaking, the non-hyperbolicity of the result-

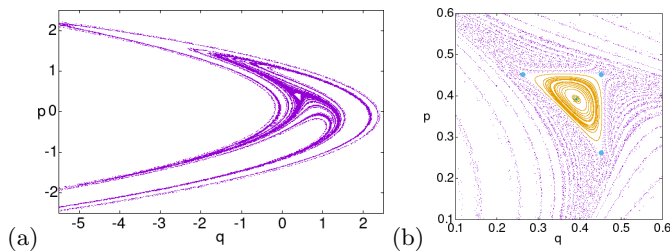


FIG. 6. (a) Unstable manifold emanating from the hyperbolic fixed point of the map (75), obtained by forward iteration of  $10^6$  initial conditions until time  $t = 15$ . (b) Marginally stable fixed point, surrounded by a stability island, triangularly shaped by an outer period-three unstable periodic orbit (blue points).

ing noisy system should introduce a continuous component in the spectrum of the transport operators and thus break the assumption of a solely discrete spectrum. However, if we investigate timescales of the order of- or shorter than the inverse escape rate from the region of the chaotic saddle, when the discrete part of the spectrum is dominant, the contribution of the continuous part of the spectrum may be ignored, due to the smallness of the stability island. Unlike for the cat map, the leading eigenfunctions of the transfer operators for the Hamiltonian Hénon map are not uniform distributions (Fig. 7(a-b)), and, due to the finite escape rate, they are conditionally invariant densities. As a consequence, we should expect from the predictions (44) and (52) that the nonequilibrium profiles of integrated observables follow the ratio of the first subleading- to the leading eigenfunction of  $\mathcal{L}_t$  ( $\mathcal{L}_t^\dagger$ ).

The theory is tested for two observables, that is the finite-time Lyapunov exponent, as well as the diffusivity

$$\hat{D}^t(x) = \frac{1}{t} \sum_{\tau=0}^t [q^2(f^\tau(x)) + p^2(f^\tau(x))]. \quad (76)$$

The density plots in Fig. 8 corroborate the expectations for the two integrated observables to be supported on the stable manifold of the map when pinned by the initial points of the iteration  $x_0 \rightarrow f^t(x_0)$  plus weak noise, and to mimic the ratio between the second and the first eigenfunction of the Koopman operator.

On the other hand, the same observables pinned by the final points of each phase-space trajectory  $f^{-t}(x_t) \rightarrow x_t$  plus weak noise are supported on the unstable manifold of the map (Fig. 9), and behave similarly to the ratio of the second to the first eigenfunction of the Perron-Frobenius operator. In both ‘forward’ and ‘backward’ pictures, the strongly chaotic phase (in orange) is distinguishable from the non-hyperbolic, weakly chaotic phase (in blue) of a three-lobed shape with tapered ends, due to a period-three unstable periodic orbit that rules the dynamics just outside the stability island (Fig. 6(b)).

Figures 8(a)-(b) and 9(a)-(b) show that the phase-space profiles of the two observables are nearly identi-

cal, and their ratios (Figs. 8(d) and 9(d)) are very close to be uniform, except for deviations visible in the non-hyperbolic region.

The white color in Figs. 8-9(a)-(b) indicates the region of the phase space where forward (Fig. 8) or backward (Fig. 9) trajectories escape from the domain examined before the time  $t$  of integration. In Figs. 8-9(c), instead, the ratio between the eigenfunctions is not defined in the blank region, where the leading eigenfunction vanishes.

The density plots of the leading- and subleading eigenfunctions of the transport operators (Fig. 7) taken separately, bear significant differences from those of the observables: the first eigenfunctions clearly describe a longer timescale than that of the observables profiles, at which noisy trajectories have mostly left the hyperbolic region, while they only survive in and around the stability island; the second eigenfunctions alone are more resemblant of the finite-time integrated observables, except they are suppressed on a ring around the stability island. That pattern is not detected in the density plots of the observables. Therefore, it does appear as though the latter are best described by the ratio  $\phi_1/\phi_0$  ( $\varphi_1/\varphi_0$ ).

### 3. Ikeda map

Let me now consider the Ikeda map

$$\begin{aligned} q' &= c_0 + c_2 q \cos \theta - c_2 p \sin \theta \\ p' &= c_2 q \sin \theta + c_2 p \cos \theta, \end{aligned} \quad (77)$$

with  $\theta = c_1 - \frac{c_3}{1+q^2+p^2}$ , while the parameters are set to  $c_0 = 1$ ,  $c_1 = 0.4$ ,  $c_2 = 0.9$ ,  $c_3 = 6$ . The Ikeda map with these parameters features a strange attractor, that is the closure of the unstable manifold of the fixed point at  $x_s \simeq (0.5228, 0.2469)$  (inverse saddle). The basin of attraction of the strange attractor is bounded by the stable and unstable manifolds of the hyperbolic fixed point  $x_h \simeq (1.1142, -2.2857)$  [32].

The Ikeda map is dissipative, and thus it does not preserve areas in the phase space, which are instead shrunk by the evolution. This phenomenon is known as squeezing, and it adds to the stretching and folding already seen in the previous Hamiltonian examples, but now plays a central role.

The first consequence of squeezing would be a strange attractor with a non-smooth measure, that emerges at long times. In order to avoid fractal measures in the phase space, that would prevent the present theory from applying, Gaussian, uncorrelated, and isotropic noise of amplitude  $2\sigma^2 = 0.025$  is added to the dynamics (77). Collaterally, some noisy orbits may now cross the stable manifold of the fixed point  $x_h$ , and exit the region of the strange attractor, which produces a tiny but non-zero escape rate.

The second effect of squeezing is a complex-conjugate pair of second eigenvalues for the transport operators, instead of the real and isolated single eigenvalue encountered in the previous Hamiltonian models. The second

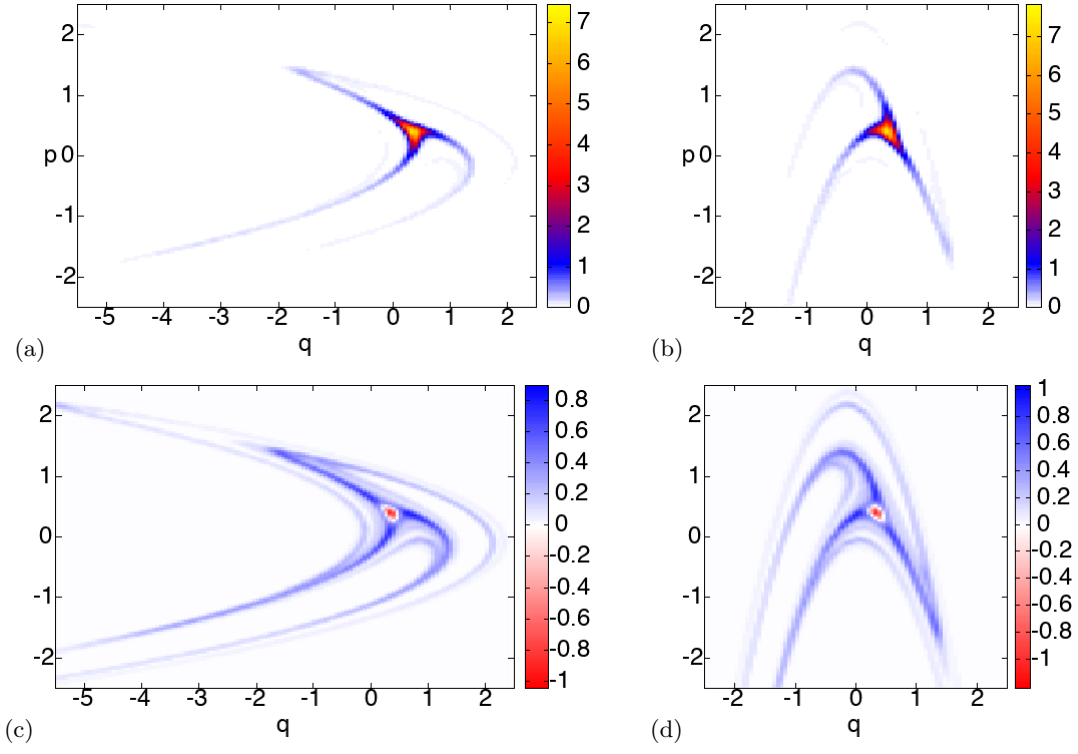


FIG. 7. (a-b): Leading eigenfunctions of the (a) Perron-Frobenius- and (b) Koopman operator for the Hénon map. (c-d): First subleading eigenfunctions of the same operators, respectively. The Ulam matrix has size  $2^{14} \times 2^{14}$ .

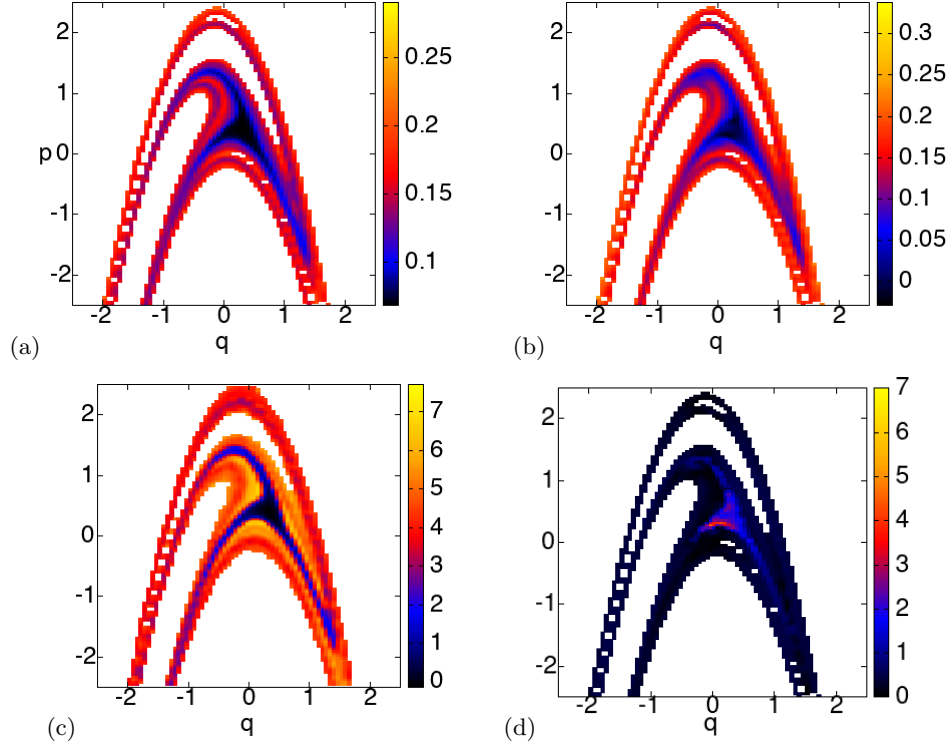


FIG. 8. (a): Phase-space density plot ( $2^{14}$  points, each averaged over  $10^4$  trajectories) of the diffusivity (76) for the Hénon map, pinned by the initial points, after  $t = 10$  iterations of the map. (b): The finite-time Lyapunov exponents,  $t = 10$ . (c) Ratio of the first subleading- to the leading eigenfunction of the Koopman operator for the same map. (d) ratio of (a) to (b), as defined in (74).

eigenvalue of the Perron-Frobenius operator yields the decay rate of any initial density to the natural measure



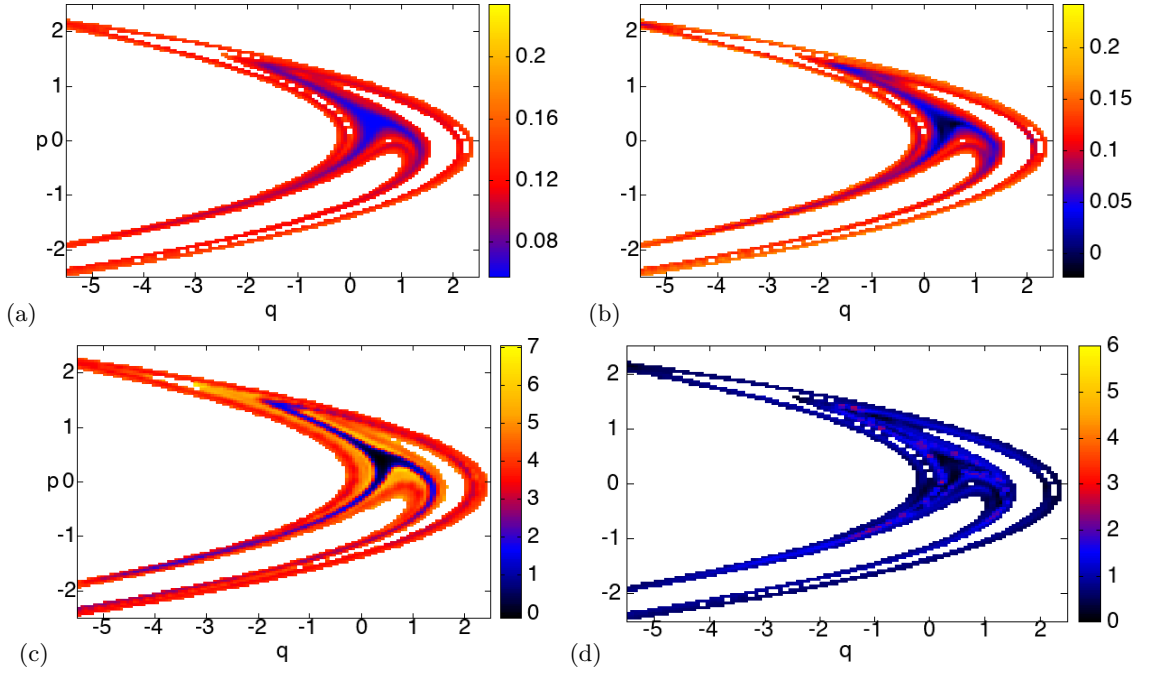


FIG. 9. (a): Phase-space density plot ( $2^{14}$  points, each averaged over  $10^4$  trajectories) of the diffusivity (76) for the Hénon map, pinned by the final points, after  $t = 10$  iterations of the map. (b): Distribution of the finite-time Lyapunov exponents,  $t = 10$ . (c) Ratio of the first subleading- to the leading eigenfunction of the Perron-Frobenius operator for the same map. (d) ratio of (a) to (b), as defined in (74).

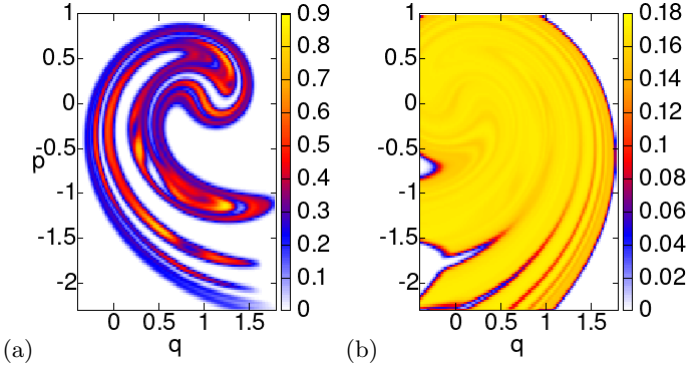


FIG. 10. First eigenfunctions of the (a) Perron-Frobenius- and (b) Koopman operator for the Ikeda map with additive noise of amplitude  $\sigma^2 = 2.5 \cdot 10^{-3}$ . The Ulam matrix has size  $2^{14} \times 2^{14}$ .

of the phase space, which can be estimated from the autocorrelation function

$$C(t) = \frac{\int w(x) [\mathcal{L}_t w](x)}{\int w^2(x)}. \quad (78)$$

Here  $C(t)$  is computed for an initial Gaussian density centered at the fixed point of the map, transported by the Ulam matrix  $\mathbf{L}^t$ , which approximates  $\mathcal{L}_t$ , and plotted as a function of time in Fig. 11(f), where it can be clearly seen to oscillate while decaying. A non-trivial imaginary part of the first subleading eigenvalue of the Perron-Frobenius/Koopman operator signals oscillations

in the decay of correlations, produced by the alternate effects of stretching, folding, and especially squeezing (Figs. 11(a)-(e)) that creates accumulation regions, unlike in the previous Hamiltonian models, where correlations decay monotonically (Fig. 11(f)).

With that observation, let us look once more at the first non-trivial term in the expansion (44) of the integrated observable  $A^t(x_0)$ :

$$\varphi_1(x_0) e^{-\gamma_1 t} \int dx \phi_1(x) A^t(f^{-t}(x)) \quad (79)$$

is now made of three complex factors, and adds up to a real number with the mirror term of  $\varphi_1^*(x_0)$  and  $\phi_1^*(x_0)$ . In that process, the combination of  $\varphi_1(x_0)$  and  $\varphi_1^*(x_0)$  gets to depend on  $\int dx \phi_1(x) A^t(f^{-t}(x))$  and its complex conjugate, which are observable specific. That in fact determines the breakdown of the universal behavior of the finite-time integrated observables predicted by the theory and exemplified in the previous models. For the Ikeda map, one should not expect distinct observables to share the same profile, as they are supposed to follow different linear combinations of the real and imaginary parts of the first subleading eigenfunctions (divided by the natural measure), all observable dependent.

In order to verify that, the density plots in Figs. 12(a)-(b) and 13(a)-(b) compare two distinct integrated observables, that is the diffusivity  $\hat{D}^t(x)$  defined as in Eq. (76), and the finite time Lyapunov exponent, defined in Eq. (24). This time the directly computed observables are both supported on and striated along the unstable

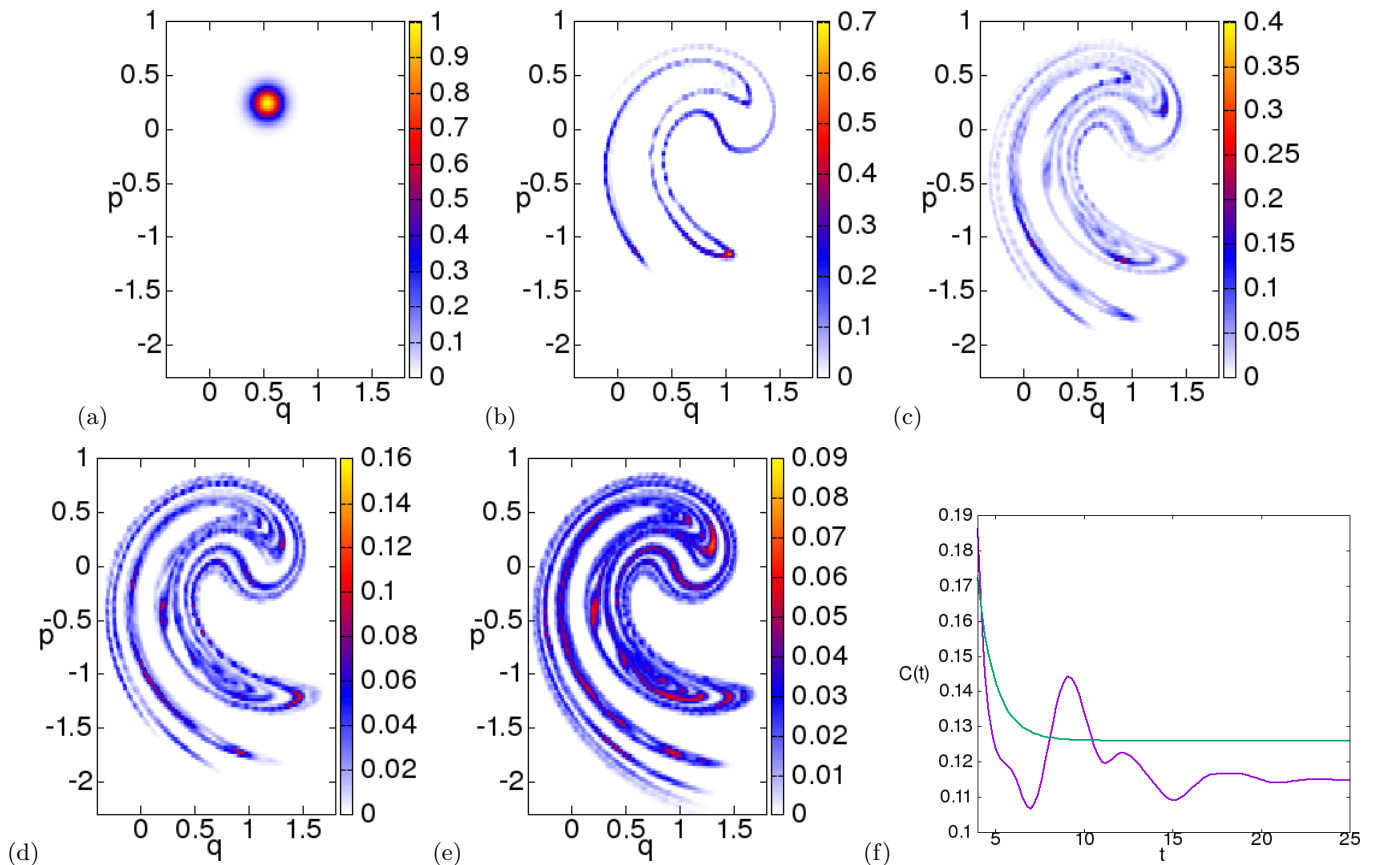


FIG. 11. Snapshots of the evolution of the initial Gaussian density centered at the fixed point  $x_s \simeq (0.533, 0.247)$ , portrayed in (a), by the Ulam matrix of the Ikeda map with noise of amplitude  $\sigma^2 = 4 \cdot 10^{-4}$ , given by the resolution; (b)  $t = 5$ ; (c)  $t = 9$ ; (d)  $t = 11$ ; (e)  $t = 25$ . (f) (purple) autocorrelation function of the initial density in (a) with the iterates at an intermediate timescale; (green) autocorrelation function of a density initially centered at the fixed point of the perturbed cat map, for comparison. The Ulam matrix has size  $2^{12} \times 2^{12}$ .

(Fig. 12) and stable (Fig. 13) manifolds respectively, but they share limited similarities.

In particular, certain features that belong now to the real- now to the imaginary part of the second eigenfunction (divided by the first, that is real valued, Figs. 12(d)-(e) and 13(d)-(e)) may be visible in the profiles of either observable (Figs. 12(a)-(b) and 13(a)-(b)), but not in a consistent manner, as seen for the non-dissipative models of the previous sections.

The ratios  $r(x, t)$ , as defined in (74), between the two integrated observables (Figs. 12(c) and 13(c)) are also striated along the manifolds, meaning that they are no longer uniform distributions with fluctuations. That indeed gives an additional indication that distinct integrated observables produce different phase-space profiles.

## V. SUMMARY

I have carried out an attempt to take the thermodynamic formalism of chaotic dynamics out of statistical equilibrium. The time evolution of the phase space is treated as a thermodynamic ensemble, and the single

chaotic trajectories as its subsystems. The probability for the value of a given observable on a trajectory follows the usual Gibbs expression, which however now includes a time-dependent statistical weight for each orbit.

With those premises, the familiar expressions relating Rényi (e. g. information) entropy, a free energy ('topological pressure'), and ensemble averages, are extended to chaotic processes that have yet to relax to statistical equilibrium.

The most notable byproduct of the present construction emerges from the evaluation of the ensemble average of an integrated observable. According to the theory, every such expectation value does depend explicitly on a phase-space weight distribution, which in turn depends both on time and, crucially, on the initial conditions. That makes average and higher moments not so meaningful by themselves, and so one rather studies the behavior of the full phase-space profiles of an integrated observable, which are found to be determined by the first two eigenfunctions of the transport (Perron-Frobenius or Koopman) operator, at an intermediate timescale during relaxation. This outcome, and the prediction of a universal behavior for the profile, is obtained with an al-



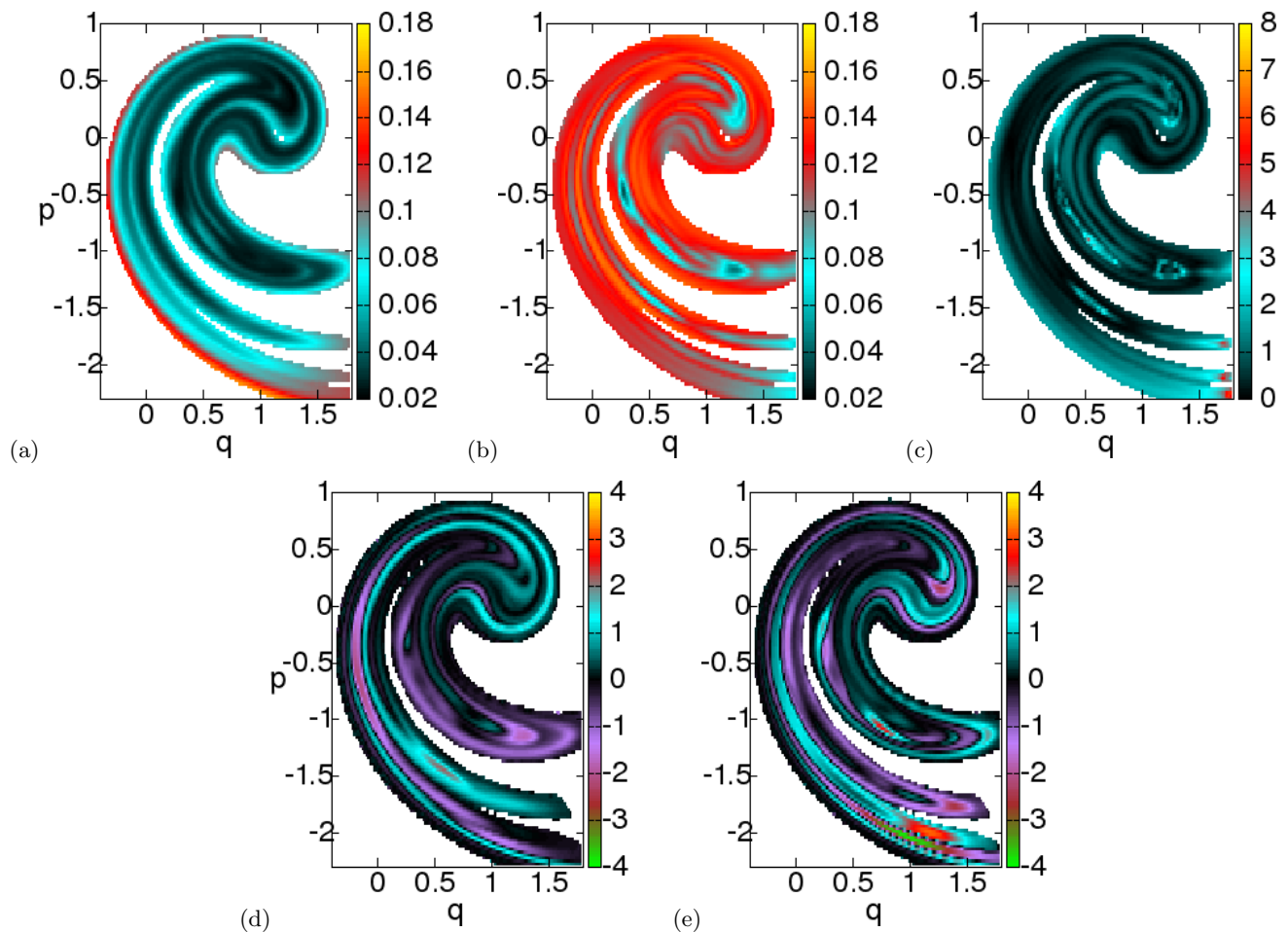


FIG. 12. (a): Density plot ( $2^{14}$  points, each averaged over  $10^4$  trajectories) of the diffusivity for the Ikeda map with noise of amplitude  $2\sigma^2 = 2.5 \cdot 10^{-3}$ , pinned by the final points, after  $t = 8$  iterations of the map. (b): Distribution of the finite-time Lyapunov exponents,  $t = 8$ . (c): Ratio of (b) to (a), as defined in (74). (d)-(e): Real- and imaginary parts respectively of the second eigenfunction of the Perron-Frobenius operator, divided by the first eigenfunction.

ternative approach to that of dynamical averages, used for both pointwise- and integrated observables in a recent report [33], and thus independently confirms the conclusions of the present work.

However, the present results are subject to a number of assumptions, and thus limitations. First, the theory is here formulated in discrete time, and thus an extension to continuous-time flows is in order. Secondly, in order for the observations on the eigenfunctions to apply, the dynamics must allow for a transport operator with a discrete spectrum, and a spectral gap. Typically, that occurs with a strongly chaotic (‘hyperbolic’) phase space, or, as seen for the Hamiltonian Hénon map, a chaotic repeller bearing a small stability island, and an appropriate choice of the functional space. Finally, the universality of the observable phase-space profiles breaks down when the second eigenvalue of the transport operator is a complex conjugate pair instead of a real-valued singlet. This is ascribed to the phase-space squeezing caused by dissipation, manifest for example in strange attractors.

The present approach to finite-time thermodynamic

formalism proves self-consistent when I formally identify the weights of the out-of-equilibrium Gibbs probabilities with phase-space densities, which are pushed forward or pulled back by well-known transport operators. Moreover, physically meaningful expressions for the ensemble averages are recovered, and the predictions for the observables in the phase space are corroborated by numerics. Yet, I did not provide a mathematically rigorous theory akin to that already existing for chaotic systems at statistical equilibrium, where, for instance, it is proved that the conventional Gibbs probabilities extremize the topological entropy. Future developments of the present theory should then move in that direction, possibly leveraging variational principles for systems out of equilibrium, such as Maximum Caliber [34], besides the mentioned need for a continuous-time formulation.

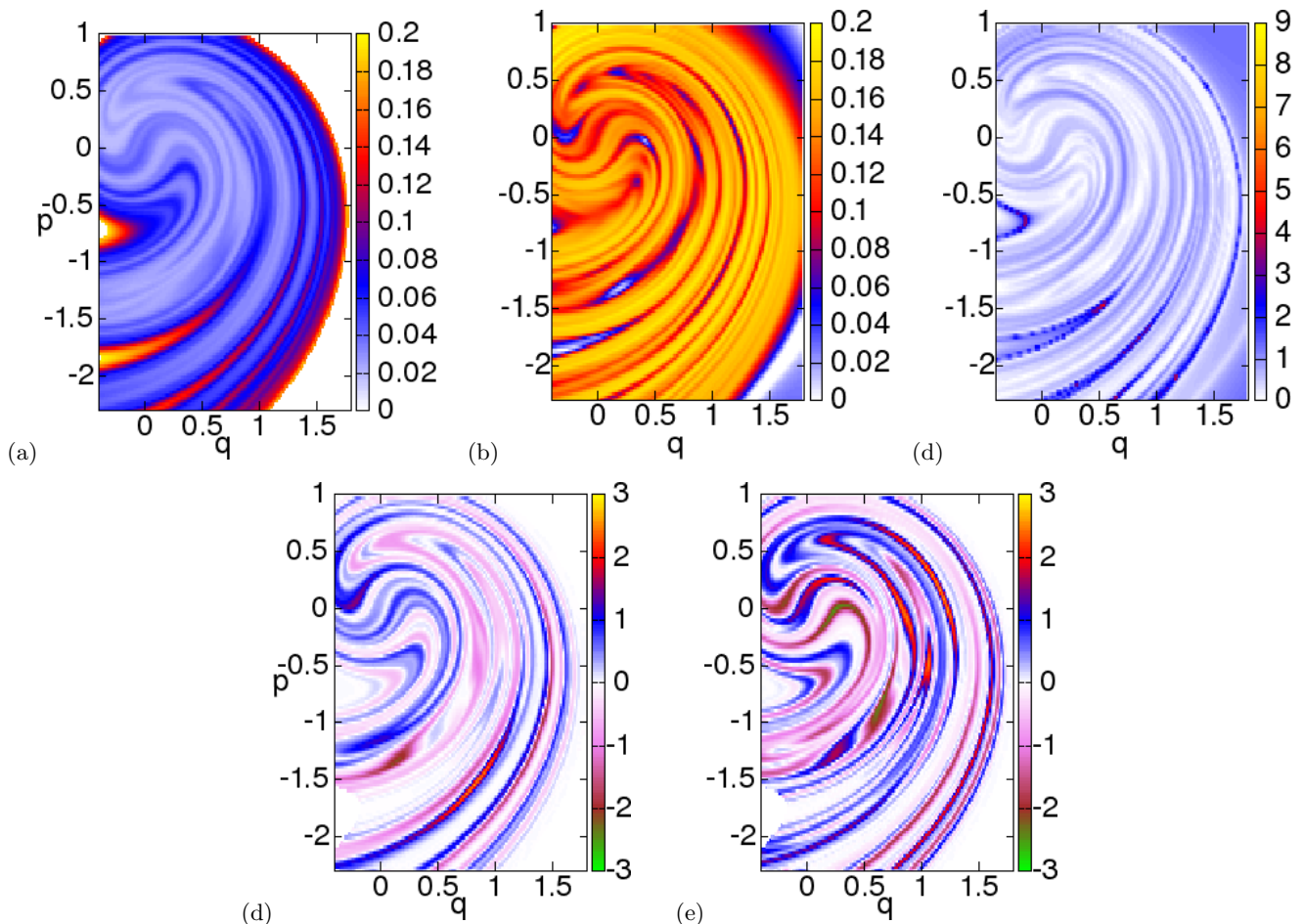


FIG. 13. (a): Density plot ( $2^{14}$  points, each averaged over  $10^4$  trajectories) of the diffusivity for the Ikeda map with noise, pinned by the initial points, after  $t = 8$  iterations of the map. (b): Distribution of the finite-time Lyapunov exponents,  $t = 8$ . (c): Ratio of (b) to (a), as defined in (74). (d)-(e): Real- and imaginary parts respectively of the second eigenfunction of the Koopman operator, divided by the first eigenfunction.

### Appendix A: Asymptotic limit for the $I_t, \mathcal{P}_t, \langle A^t \rangle$ thermodynamic relation

Let us retrieve Eq. (10), relating information entropy, topological pressure, and expectation value of an integrated observable at equilibrium, from the limit  $t \rightarrow \infty$  of its finite-time, non-equilibrium counterpart (23) derived in Sec. II.

An argument may be used from Reference [2] to help determine the asymptotic behavior of our finite-time thermodynamic relation connecting Shannon information, Gibbs average, and topological pressure. Take as integrated observable  $A^t = \ln |\Lambda(t)|$ , the finite-time Lyapunov exponent, as defined in Sec. II, Eq. (24). Consider the partition function

$$Z_t(\beta) = - \sum_j \frac{w_j(t)}{|\Lambda_j(t)|^\beta}. \quad (\text{A1})$$

Assume that all the weights  $w_j$  are bounded by positive constants  $c_1$ , and  $c_2$  as

$$c_1 \leq w_j \leq c_2. \quad (\text{A2})$$

That is reasonable, if the map in question is expanding or hyperbolic, since in that case the dynamics is everywhere unstable and no trajectory/sequence may ever carry infinite statistical weight. We may then sandwich the partition function (A1) as

$$c_1 \sum_j \frac{1}{|\Lambda_j(t)|^\beta} \leq \sum_j \frac{w_j(t)}{|\Lambda_j(t)|^\beta} \leq c_2 \sum_j \frac{1}{|\Lambda_j(t)|^\beta}, \quad (\text{A3})$$

and hence

$$\begin{aligned} \frac{1}{t} \ln c_1 \sum_j \frac{1}{|\Lambda_j(t)|^\beta} &\leq \frac{1}{t} \ln \sum_j \frac{w_j(t)}{|\Lambda_j(t)|^\beta} \leq \frac{1}{t} \ln c_2 \sum_j \frac{1}{|\Lambda_j(t)|^\beta} \\ \frac{1}{t} \ln c_1 + \frac{1}{t} \ln \sum_j \frac{1}{|\Lambda_j(t)|^\beta} &\leq \frac{1}{t} \ln \sum_j \frac{w_j(t)}{|\Lambda_j(t)|^\beta} \leq \frac{1}{t} \ln c_2 + \frac{1}{t} \ln \sum_j \frac{1}{|\Lambda_j(t)|^\beta}, \end{aligned} \quad (\text{A4})$$

so that, when  $t \rightarrow \infty$ , both inequalities saturate to yield the same expression

$$\lim_{t \rightarrow \infty} \frac{1}{t} \ln \sum_j \frac{1}{|\Lambda_j(t)|^\beta} = \mathcal{P}(\beta). \quad (\text{A5})$$

This is the topological pressure defined at equilibrium with the unweighed Gibbs probabilities, whose ensemble constitutes the pointwise natural measure of the dynamical system at hand [3]. Besides retrieving  $\mathcal{P}(\beta)$  from the  $t \rightarrow \infty$  limit of  $\mathcal{P}_t(1, \beta)$ , the previous analysis tells us that the quantity  $Z_t(\beta)$  given by Eq. (A1) is also bounded as, say,  $c'_1 \leq Z_t(\beta) \leq c'_2$ .

Let us now apply the same idea as in (A3) to the tilted information  $S_t(\beta)$ : let

$$\chi_1 \leq w_j \ln w_j \leq \chi_2, \quad (\text{A6})$$

for some  $\chi_1, \chi_2$ , and so

$$\chi_1 \sum_j \frac{1}{|\Lambda_j(t)|^\beta} \leq \sum_j \frac{w_j(t) \ln w_j(t)}{|\Lambda_j(t)|^\beta} \leq \chi_2 \sum_j \frac{1}{|\Lambda_j(t)|^\beta}, \quad (\text{A7})$$

that also results in upper and lower bounds for  $t S_t(\beta)$ . Then we may also sandwich the ratio  $t S_t(\beta)/Z_t(\beta)$  we have encountered in Eq. (23):

$$\frac{\chi'_1}{c'_2} \leq \frac{\sum_j \frac{w_j(t) \ln w_j(t)}{|\Lambda_j(t)|^\beta}}{\sum_j \frac{w_j(t)}{|\Lambda_j(t)|^\beta}} \leq \frac{\chi'_2}{c'_1}, \quad (\text{A8})$$

with the assumption that  $w_j(t) > 0$ . The previous bounds are constant in time, and thus, including the factor of  $1/t$  originally in Eq. (23), we have that

$$\lim_{t \rightarrow \infty} \frac{S_t(\beta)}{Z_t(\beta)} = \lim_{t \rightarrow \infty} \frac{1}{t} \frac{\sum_j \frac{w_j(t) \ln w_j(t)}{|\Lambda_j(t)|^\beta}}{\sum_j \frac{w_j(t)}{|\Lambda_j(t)|^\beta}} = 0, \quad (\text{A9})$$

and Eq. (23) does reduce to the steady-state thermo-

dynamic relation (13) linking information entropy, Lyapunov exponent, and escape rate (for  $\beta = 1$ ).

## Appendix B: Eigenfunction expansion for backward evolution

Let me here provide the intermediate steps leading from Eq. (51) to Eq. (52). First, in the left-hand side of Eq. (51), I expand  $[\mathcal{L}_t^\dagger w](x)$  in terms of the eigen-spectrum of the Koopman operator, to obtain for the expectation  $\langle A^t \rangle$ :

$$\langle A^t \rangle_\beta = \frac{\sum_n \tilde{b}_n e^{-\gamma n t} \int dx \varphi_n(x) A^t(x) e^{-\beta A^t(x)}}{\sum_n \tilde{b}_n e^{-\gamma n t} \int dx \varphi_n(x) e^{-\beta A^t(x)}}, \quad (\text{B1})$$

with

$$\tilde{b}_n = \int dy w(y) \phi_n(y). \quad (\text{B2})$$

As before with the  $\varphi_n(x)$ , this time the eigenfunctions  $\phi_n(x)$  of the Perron-Frobenius operator are hidden in the coefficients  $\tilde{b}_n$  of the expansion, and yet they come out when we take a density pinned at a definite point,  $w(x) = \delta(x - x_t)$ . Then the average of the integrated observable becomes the phase-space function

$$\langle A^t \rangle_{\beta=0}(x_t) = \frac{\int dx A^t(x) \int dy \delta(y - f^t(x)) \delta(y - x_t)}{\int dx \int dy \delta(y - f^t(x)) \delta(y - x_t)} = \frac{A^t(f^{-t}(x_t))}{|\det J^t(f^{-t}(x_t))| \mu(\mathcal{M}(t))}. \quad (\text{B3})$$

Specularly to Eq. (42), I obtain for  $\hat{A}^t(f^{-t}(x_t))$  in terms of the spectral expansion,

$$\hat{A}^{-t}(x_t) := \langle A^t \rangle_{\beta=0}(x_t) = \frac{\sum_n \phi_n(x_t) e^{-\gamma n t} \int dx \varphi_n(x) A^t(x)}{\sum_n \phi_n(x_t) e^{-\gamma n t} \int dx \varphi_n(x)}. \quad (\text{B4})$$

The meaning of the previous expression is that the pointwise expectation of any integrated observable pinned by

the *arrival* point  $x_t$  in the phase space is a superposition of eigenfunctions of the Perron-Frobenius operator.

The truncation (44) to the second eigenfunction may also

be applied here to Eq. (B4), for timescales of the order  $(\gamma_1 - \gamma_0)^{-1}$ , and it results in Eq. (52).

- 
- [1] R. Bowen, *Equilibrium States and the Ergodic Theory of Anosov Diffeomorphisms*, Springer, 1975.
- [2] C. Beck and F. Schlögl, *Thermodynamics of Chaotic Systems*, Cambridge, 1997.
- [3] P. Gaspard, *Chaos, Scattering, and Statistical Mechanics*, Cambridge, 1998.
- [4] D. Ruelle, *Thermodynamic Formalism: The Mathematical Structure of Equilibrium Statistical Mechanics*, Cambridge, 2004.
- [5] H. Touchette, The large deviation approach to statistical mechanics, Phys. Rep. **478**, 1-69 (2009).
- [6] P. Cvitanović, R. Artuso, R. Mainieri, G. Tanner and G. Vattay, *Chaos: Classical and Quantum*, ChaosBook.org (Niels Bohr Institute, Copenhagen 2020).
- [7] J. Slipantschuk, O. F. Bandtlow, and W. Just, Symmetry decomposition of chaotic dynamics, J. Phys. A: Math. Theor. **46**, 075101 (2013).
- [8] N. R. Smith, Large deviations in chaotic systems: exact results in dynamical phase transitions, Phys. Rev. E **106**, L042202 (2022).
- [9] R. Gutiérrez, A. Canella-Ortiz, and C. Pérez-Espigares, Finding the Effective Dynamics to Make Rare Events Typical in Chaotic Maps, Phys. Rev. Lett. **131**, 227201 (2023).
- [10] C. Monthus, Large deviations and conditioning for chaotic non-invertible deterministic maps: analysis via the forward deterministic dynamics and the backward stochastic dynamics, J. Stat. Mech. 013208 (2024).
- [11] H. Kantz and P. Grassberger, Repellers, semi-attractors, and long-lived chaotic transients, Physica D **17**, 75 (1985).
- [12] D. Chandler, *Introduction to Modern Statistical Mechanics*, Oxford, 1987.
- [13] According to reference [2], the quantity to be minimized is the function  $\Psi_t(a, p) = \sum_j p_j \beta E_j + p_j \ln p_j$ .
- [14] J. P. Eckmann and D. Ruelle, Ergodic theory of chaos and strange attractors, Rev. Mod. Phys. **57**, 617.
- [15] R. Chetrite and H. Touchette, Nonequilibrium microcanonical and canonical ensembles and their equivalence, Phys. Rev. Lett. **111**, 120601 (2013).
- [16] R. Chetrite and H. Touchette, Nonequilibrium Markov processes conditioned on large deviations, Ann. Henri Poincaré **16**, 2005 (2015).
- [17] I assume the flow  $f^t$  to be invertible, so there is a 1 – 1 correspondence between every  $x$  and  $f^{-t}(x)$ .
- [18] A. Lasota and M. MacKey, *Chaos, Fractals, and Noise; Stochastic Aspects of Dynamics*, Springer, New York, 1994.
- [19] D. Lippolis, A. Shudo, K. Yoshida, and H. Yoshino, Scarring in classical chaotic dynamics with noise, Phys. Rev. E **103**, L050202 (2021).
- [20] K. Yoshida, and H. Yoshino, A. Shudo, and D. Lippolis, Eigenfunctions of the Perron-Frobenius operator and the finite-time Lyapunov exponents in uniformly hyperbolic area-preserving maps, J. Phys. A: Math. Theor. **54**, 285701 (2021).
- [21] P. Cvitanović and D. Lippolis, Knowing when to stop: How noise frees us from determinism, AIP Conf. Proc. **1468**, 82 (2012).
- [22] D. J. Driebe, *Fully Chaotic Maps and Broken Time Symmetry*, Springer, Dodrecht, 1999.
- [23] R. F. Fox, Construction of the Jordan basis for the Baker map, Chaos **7**, 254 (1997).
- [24] D. J. Chappell and G. Tanner, Solving the stationary Liouville equation via a boundary element method, J. Comp. Phys. **234**, 487 (2013).
- [25] G. Froyland, On Ulam approximation of the isolated spectrum and eigenfunctions of hyperbolic maps, Discr. Cont. Dyn. Syst. **17**, 671 (2007).
- [26] F. Brini, S. Siboni, G. Turchetti, and S. Vaienti, Decay of correlations for the automorphism of the torus  $\mathbb{T}^2$ , Nonlinearity **10**, 1257 (1997).
- [27] M. Blank, G. Keller, and C. Liverani, Ruelle-Perron-Frobenius spectrum for Anosov maps, Nonlinearity **15**, 1905 (2002).
- [28] S. M. Ulam, *A Collection of Mathematical Problems* (Interscience, New York, 1960).
- [29] L. Ermann and D. L. Shepelyansky, The Arnold cat map, the Ulam method, and time reversal, Physica D **241**, 514 (2012).
- [30] V. I. Arnold and A. Avez, *Ergodic Problems of Classical Mechanics*, Benjamin, New York, 1968.
- [31] Here the evolution operators are approximated with matrices, meaning that the numerically computed normalized eigenvectors are determined up to a sign. In any case the  $\varphi_n$  must be bi-orthogonal to the  $\phi_n$ , while the  $A^t(f^{-t}(x))$  considered here are positive definite, hence the sign of  $\varphi_n$  determines the sign of the integral  $\int dx \phi_n(x) A^t(f^{-t}(x))$  as well.
- [32] G. Osipenko, *Dynamical Systems, Graphs, and Algorithms*, Springer, 2007.
- [33] D. Lippolis, Chaotic fields behave universally out of equilibrium, arXiv:2402.11976.
- [34] P. D. Dixit, J. Wagoner, C. Weistuch, S. Pressé, K. Ghosh and K. A. Dill, Maximum caliber is a general variational principle for dynamical systems, J. Chem. Phys. **148**, 010901 (2018).